The Safety and Tolerability of Nanoparticles for Neurological Disease Applications

A thesis submitted in partial fulfilment of the

HONOURS DEGREE of BACHELOR OF

HEALTH AND MEDICAL SCIENCES In

The Discipline of Anatomical Sciences

Adelaide Medical School

The University of Adelaide

By Laura Carr

November 2020

Abstract

Neurological disorders, such as Parkinson's disease (PD), are a significant problem globally, the leading cause of disability and the second leading cause of death. Currently, treatment of PD involves alleviating symptoms, as targeting disease mechanisms is difficult due to the blood brain barrier. Nanoparticle (NP) assisted drug delivery has high biomedical promise and nanoparticles have been investigated for use in the central nervous system (CNS). However, the safety of NPs in the CNS is not well defined and involves understanding the neuroinflammatory response regulated by microglia, which may exist in altered states in neurological disorders. The research presented here characterised microglial number and activation state in PD, and assessed the toxicity and ability to induce neuroinflammatory responses of gold nanoparticles (GNPs) or carbon nanotubes (CNTs) when administered to a microglia-like cell line (BV-2). Microglial number was higher in the striatum and substantia nigra of the brain compared to pre-frontal and hippocampus, but no differences were observed between control or PD brain tissue in number of total or activated microglia. BV-2 cells showed no loss of viability or increased inflammatory response after treatment with GNPs but showed a decrease in viability when treated with high doses of CNTs. Combined with LPS to model an inflammatory environment, GNPs increased but CNTs decreased IL-6 responses, suggesting GNPs may pose deleterious toxicity and inflammatory responses but CNT's may benefit a reduction in inflammation . These results present a foundation for understanding neurotoxic effects of CNTs and GNPs, and states of microglia in PD.

Word count 4958

1. Introduction

Neurological diseases (NDs) are disorders of the nervous system that affect the brain, behaviour, and cognitive ability[1]. Data from the Global Burden of Disease study 2010 (GBD 2010) showed NDs account for 3% of disability adjusted life years (DALY) and have dramatically increased over time, with NDs now the leading cause of disability worldwide and accounting for 16.5% of overall deaths[2, 3]. Neurodegenerative disorders, such as Parkinson's disease (PD) and Alzheimer's disease (AD)[4], make up a large portion of NDs and are characterised by the degeneration and functional loss of neurons . PD, one of the most common neurodegenerative disorders, currently affects 6.2 million people[1]. PD is characterised by the progressive loss of dopaminergic (DA) neurons in the substantia nigra (SN), causing a range of motor and cognitive deficits[5, 6]. Age is the biggest risk factor for developing PD, and due to population growth and aging, the burden of PD is likely to increase in the future, as will the demand for disease modifying treatments[3].

Currently, PD treatments are focused on the symptoms, rather than addressing the root cause. The 'gold standard' treatment for PD is Levodopa, a dopamine replacement drug which does not undo the neuronal loss or halt PD [7 8] and thus alternative restorative or neuroprotective treatments are needed.

In developing new treatments it is important to consider safety and ensure therapy will not worsen the neuroinflammatory processes that drive neuronal death in PD. Microglia regulate the CNS inflammatory response and[9-11] multiple studies have identified increased microglial activation and inflammatory markers in areas associated with neuronal loss in PD such as the striatum and SN[12-16]. Activated microglia release pro-inflammatory cytokines such as Interleukin-6 (IL-6) sustaining the chronic inflammatory response and contribute to neuronal damage[14]. Understanding microglial responses and states in the PD brain is crucial in developing neuroprotective treatments.

Additionally, the major obstacle for treating PD is the blood brain barrier (BBB). Restricted movement of substances across the BBB maintains a healthy CNS environment, but is problematic for drug delivery, as ~98% of small molecule drugs cannot cross the BBB and don't access the

intended sites of action[17, 18]. One potentially strategy to overcome the BBB is using nanoparticles (NPs), with features that improve potential transport into the brain at efficacious doses[19].

NPs range from 1-100nm, and are classified according to their origin/nature-organic, inorganic, or carbon based (Figure 1)[19-21]. Organic NPs are ideal for drug delivery, as they are usually non-toxic, biodegradable and have a hollow core. Inorganic NPs include metal and metal oxide nanoparticles. Carbon based NPs, including carbon nanotubes and graphene, are made solely of carbon[19, 20]. Properties of NPs that make them ideal for use in biomedicine include size, charge, surface modifiability and chemical composition[19, 22, 23]. The modifiable surface of NPs enhances the ability

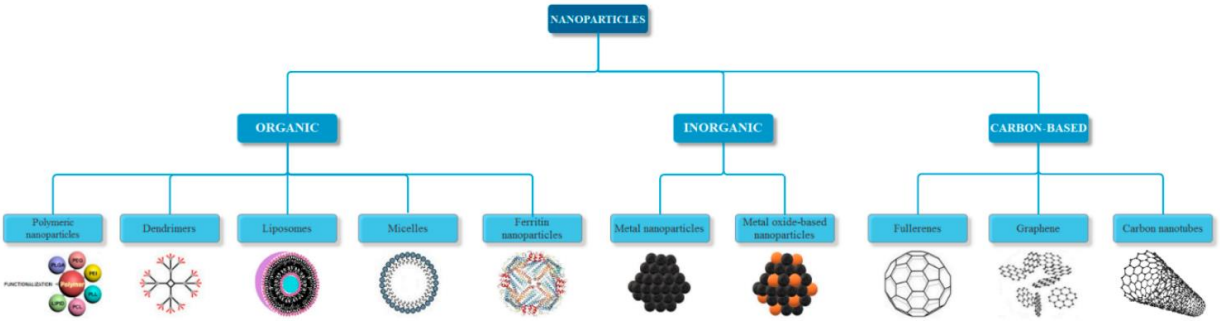

Figure 1: Schematic representation of nanoparticles classified based on their nature[11] .

to selectively target sites within the body, for instance by conjugation of antibodies to target specific regions of the brain[24], while functionalisation of NPs by surface coating may increase their tolerability within the brain [25].

One type of NPs that have been well investigated in the CNS are polymer-based particles. Chitosan NPs (a biodegradable polymer) loaded with Selegiline, a medication used to treat PD, have been administered to rats, in a PD model of rotenone-induced neuronal damage[26]. Treatment improved performance on functional tasks and significantly increased dopamine levels, with no reported cytotoxic effects. Similar polymeric nanoparticles functionalised with Anti-$A\beta_{1-42}$ reduced protein aggregations and corrected memory deficits in an *in vivo* model of AD, again with no reported cytotoxicity[27].

While polymeric nanoparticles show therapeutic promise in neurodegenerative environments this is still a developing area, particularly for long-term safety as would be required for PD therapy. Key

alternatives with good safety profiles include carbon-based nanomaterials and inorganic particles, such as GNPs. GNPs have proven applications in drug delivery and can be delivered to the brain via inhalation and transport to the olfactory nerves[28, 29]. Administration of functionalised GNPs loaded with Anthocyanin, a natural antioxidant in an *in vivo* AD model resulted in enhanced neuroprotective and anti-inflammatory effects[30]. This suggests drug-loaded GNPs can treat neurodegenerative diseases, however the literature on the safety of GNPs is mixed, with debate on toxicity. Contrastingly,, BSA functionalised GNPs evoke an irreparable toxic response in the liver and kidneys[31]. Patra et al, demonstrated variability in the toxicity of GNPs with induction of cell death in A549 human carcinoma lung cell line, but not in BHK21 (baby hamster kidney) or HepG2 (human hepatocellular liver carcinoma) cell lines[32].

Similarly, carbon nanomaterials are another class of NP showing promise in treating neurodegenerative diseases with the most common type being carbon nanotubes (CNTs). Particularly of interest to PD, CNTs have potential for neuroregeneration, where in embryonic rats, functionalised CNTs improved neuronal viability and growth, and could control neurite outgrowth[33, 34]. Similar to GNPs, CNTs cytotoxicity is reported to be dependent on cell type, with conflicting results reported[34, 35]. CNT have little effect on cell viability and inflammatory responses on peripheral cell lines or *in vivo* peripheral tumours responses[36, 37]. Contrastingly, in CNS environments, CNTs reduce cell viability, reportedly with biggest impact in cells with high phagocytic ability, such as microglia[38]. The increased response of phagocytic cells to CNTs has important implications for use in PD where microglia are highly reactive and drive pathology[39]. Therefore the effects of CNTs on these microglia is an important consideration in PD treatment development.

These studies highlight how little is understood about the impact of GNPs and CNTs on the body, particularly in the CNS environment. Since microglia are key drivers of the altered inflammatory environment seen in PD, this cell type must be specifically investigated and their responses to GNP's and CNTs assessed to define their potential as PD treatment.

We hypothesise that microglia are activated in PD and that NPs of different compositions can increase the inflammatory response and cellular viability of microglia. To address this we aimed to:

a) Characterise the total number of microglia and their activation states in the brain from PD patients; achieved by IBA1 staining of microglia in human control and PD brain tissue, and quantitation by automated counting software. Outcomes will further define the states of microglia in PD.
b) Define the capacity for GNPs and CNTs to affect viability and pro-inflammatory capacity of microglia under standard culture or in an inflammatory environment induced by LPS treatment. Outcomes will determine if GNPs or CNT's are safe candidates to take further as delivery vehicles for drugs to the PD brain.

2. Materials and methods

2.1 Tissue collection and staining

Deidentified human tissue was provided by the South Australian Brain Bank and investigations were approved by the University of Adelaide low risk human research ethics committee (H-2016-174). Examples of case records are provided in appendices a (control) and b (PD). Regions of the brain to be analysed include the areas of neuronal death (striatum and SN), and areas associated with symptoms of PD (prefrontal cortex (PFC) and hippocampus). 11 PD and 6 control cases were provided. One control case was excluded due to evidence of a conflicting inflammatory disorder, giving a total n=16. Tissue was pre-cut and immunohistochemical analysis was performed using standard protocols. Briefly, slides were deparaffinized in xylene, rehydrated in ethanol and endogenous perioxidases were blocked using methanol with 0.5% hydrogen peroxide. Slides were washed twice with PBS before antigen retrieval (citrate), and sections were blocked in 3% normal horse serum (NHS) for 30min, following incubation overnight with IBA-1 (Wako, 019-19741, 1:1000). Slides were then washed twice with PBS, incubated for 30min with secondary antibody (Vector Goat Anti-Rabbit IgG, 1:250 NHS) before washing twice with PBS and incubating for 1hr with streptavidin peroxidase conjugate (Vector SPC, 1:1000 NHS). A final wash in PBS was performed and 3,3-Diaminobenzidine tetrahydrochloride (Vector DAB; 1:50) was applied for 7 minutes. Following, slides were counterstained with haematoxylin, dehydrated in ethanol and cleared with xylene before coverslipping.

2.2 Image Analysis

Hamamatsu NanoZoomer was used to image slides. Using QuPath[40], slides were exported into tiles at 13.3xzoom for screen size 1920x1088. Tiles were excluded based on criteria that would likely impact automated count (e.g. blurry image, tissue artifacts, large vessels visible). Measure function on ImageJ[41] was used to sort images based on stain density, in groups of <40 and >40 image density. ImageJ ‘colordeconvolution’ plugin[42] was used and parameters were set with different thresholds for

each group, <40 = threshold of 0,70 and >40 = threshold of 0,80. Pixel size was kept constant at 47–2000. Procedure for activation analysis was the same, except with the addition of circularity parameters set to 0.90–1.00, in order to differentiate amoeboid/activated cells from non-activated cells with extended processes. Result tables for groups were combined and cells per mm^2 calculated for each case (total number of cells / total area). Correlational analysis was performed for regions of interest (striatum and PFC) in order to compare counts from ImageJ against HALO automated cell counting software (Indica labs, Albuquerque, New Mexico, USA) and graphed using GraphPad Prism8.

2.3 Cell culturing

Mouse microglia-like cells (BV-2) were cultured for no more than 29 passages. Culture media was Dulbecco's Modified Eagle's Medium (DMEM): high-glucose with 10% fetal bovine serum, 2nM L-Glutamine, 50U/ml Penicillin-Streptomycin, 100µg/ml Normocin. Cells were grown in a humidified incubator at 37°C with 95% air and 5% CO_2.

2.4 Nanoparticle preparation

Gold NPs (#753688, 100nm diameter, stabilised suspension in 0.1 PBS, reactant free) and Single walled carbon nanotubes (SWCNTs) (# 652490, 1.4nm ± 0.1nm, single walled carboxylic acid functionalised) were supplied by Sigma Aldrich. CNTs were prepared in Phosphate-buffered saline (PBS) at 1mg/ml and vortexed, before being subjected to ultrasonic treatment for 40 minutes prior to use in order to reduce aggregations. Both the GNPs and the CNTs were stored at 4°C.

2.5 Treatment parameters

As there is little data available on nanoparticle administration to BV-2 cells, concentrations were selected based on previous work in our laboratory for a wide assessment of viability and inflammatory response. GNPs were administered for 2hrs at 3, 30 and 300µg/mL, and 24hrs. 24hrs prior to treatments, cells were plated at 20,000 cells/well in 96 well plates and allowed to adhere. A positive

control for Interleukin-6 (IL-6) release, lipopolysaccharide (LPS), was included, along with co-treatment of nanoparticles at the upper and lower concentrations with LPS, and a vehicle control of media alone. All samples and controls were performed in triplicate and experiments independently repeated at least twice.

2.6 MTT assay for cell viability

MTT (3-(4,5-dimethylthiazol-2-yl)-2,5-diphenyltetrazolium bromide, Invitrogen, California, United States, #M6494) assays were performed using the "quick protocol" as in manufacturer's instructions. 2.4mg MTT powder was mixed with 10mL serum-free media before incubation for 2hrs. Media was replaced with 100µl dimethyl sulfoxide (DMSO) for 10 minutes before reading at 570nm.

2.7 ELISAs for assessing inflammatory response

ELISAs (enzyme-linked immunosorbent assay) were performed using supernatant from treated cells. 50µl of supernatant was used immediately and the left over stored at -20°C. Samples and standards were performed in triplicate. ELISA kits (Mouse IL-6, #555240) and equivalent reagent kits (Reagent set B #550534) were obtained from BD Biosciences (California, United States). Assays were performed in 96-well half area plates according to provided protocols, but with a 1:100 dilution of antibodies and half the volume of reactants. Sample incubation time was extended to overnight at 4°C. Standard curve was plotted and results graphed and analysed using GraphPad Prism8.

2.8 Statistical analysis

Two-way ANOVAs with Tukey's post hoc analysis and Pearson's correlational analyses were performed for cell count data. Two-way ANOVAs with Tukey's post hoc analysis were performed for ELISA and MTT data. P-values of <0.05 were considered significant.

3. Results

To understand the effects of microglia in Parkinson's disease, we took two approaches. The first to quantify the presence of inflammatory cells in human PD and the second to investigate neurotoxic responses to nanoparticles *in vitro.*

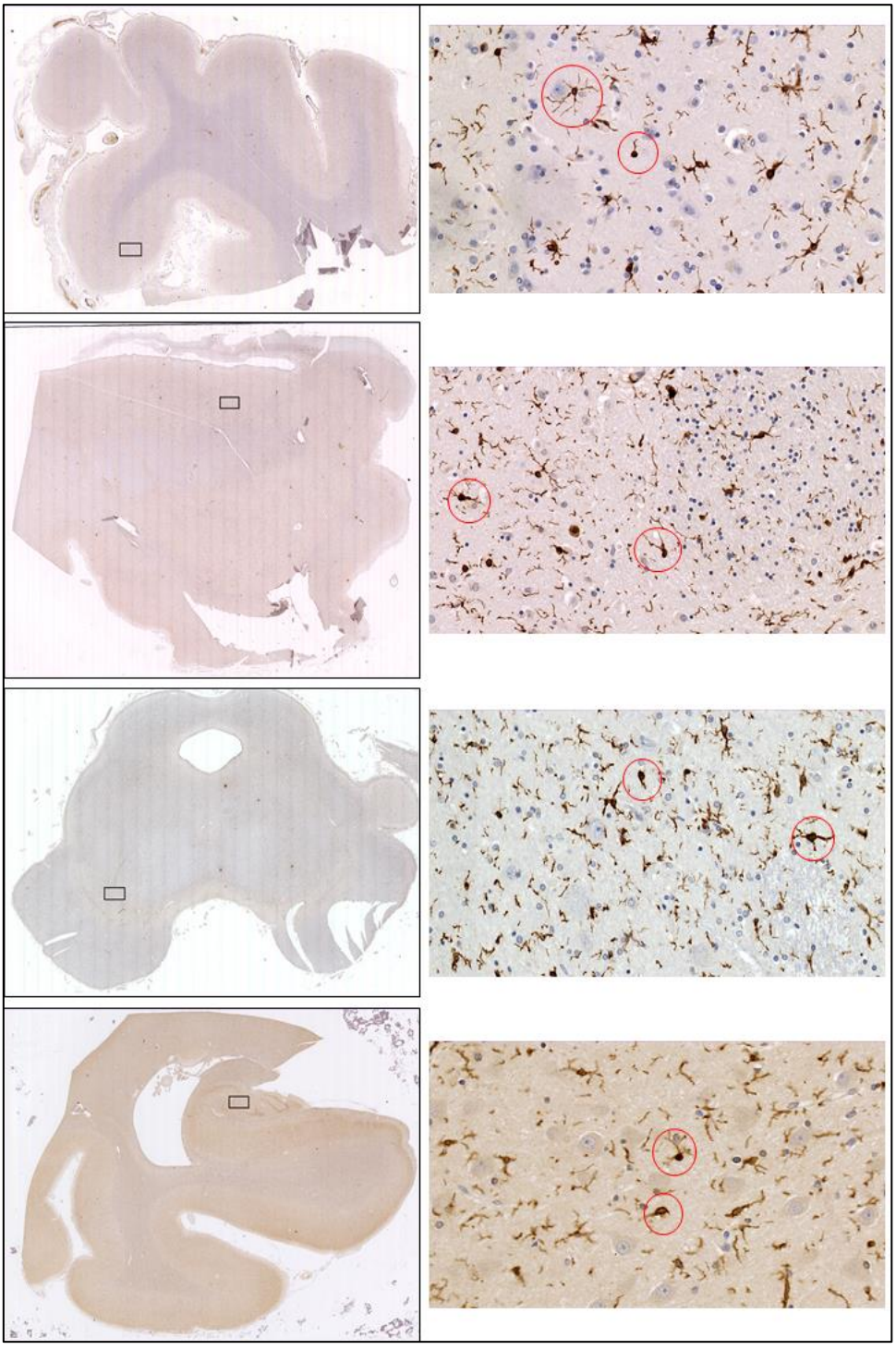

Figure 2: Representative images of regions from brain tissue stained for IBA1. a) PFC b) Striatum c) SN d) Hippocampus. Boxed regions on left image outlines the area taken for the image on the right at 40x magnification. Brown cells indicate microglia, examples are circled in red

3.1 Total Microglial counts in control and PD

Human tissue was stained for IBA1 and analysed by ImageJ. Representative images and examples of microglial cells are circled (figure 2). There was a significant main effect of region (figure 3) ($F(3,36) = 43.82$, $p < 0.0001$). Pairwise comparisons of region using the LSD method showed total number of microglia within the SN was significantly higher (136.38 (12.48)) than in the striatum (92.90 (10.89), $p < 0.001$), PFC (30.61 (6.45), $p < 0.001$) or hippocampus (42.12 (9.31), $p < 0.001$). Similarly, total number of the microglia in the striatum was higher than the PFC ($p < 0.001$) or hippocampus ($p < 0.001$). There was no significant difference between total number of microglia in the hippocampus and PFC ($p = 0.215$). Interestingly, there was no significant main effect of group ($F(1, 12) = 0.252$, $p = 0.625$). There was also no significant interaction between region and group ($F(3, 36) = 1.435$, $p = 0.248$).

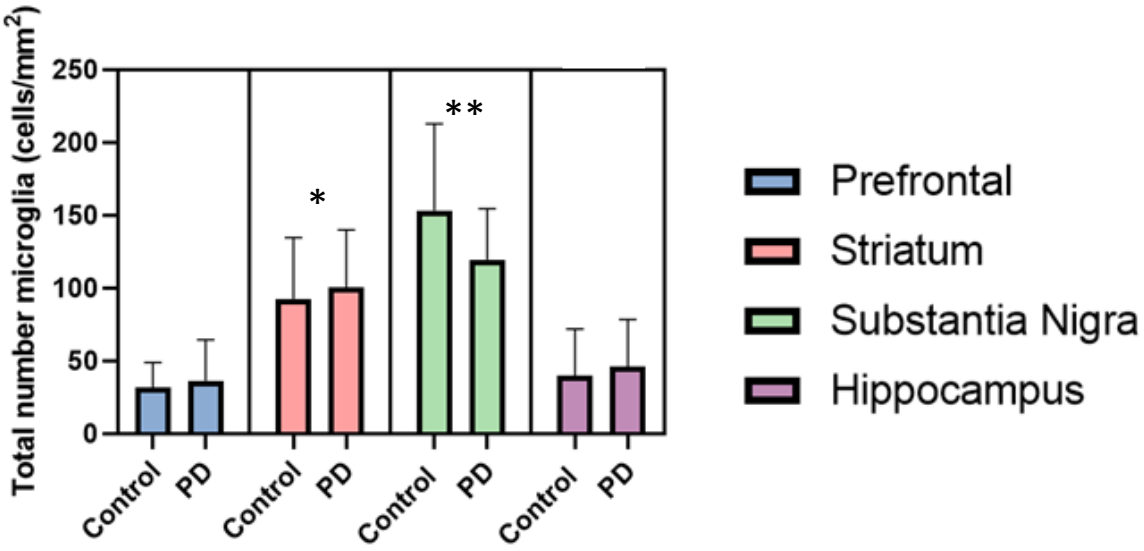

*Figure 3: Total microglia per mm² in control vs PD cohort. IBA1 positive cells were quantitated in ImageJ n=11 PD, n=5 control. Data was analysed by two-way ANOVA. No significant differences were observed between control and PD within each region. */** = significantly different to other regions*

Analysis was performed independently using HALO in order to validate ImageJ counts. Counts were compiled in excel (appendix c). Correlational analyses were performed in the PFC (r=0.96, p=<0.0001) (Figure 4a) and striatum (p=<0.0001, r=0.90) (Figure 4b), where significant correlations between ImageJ and HALO were observed.

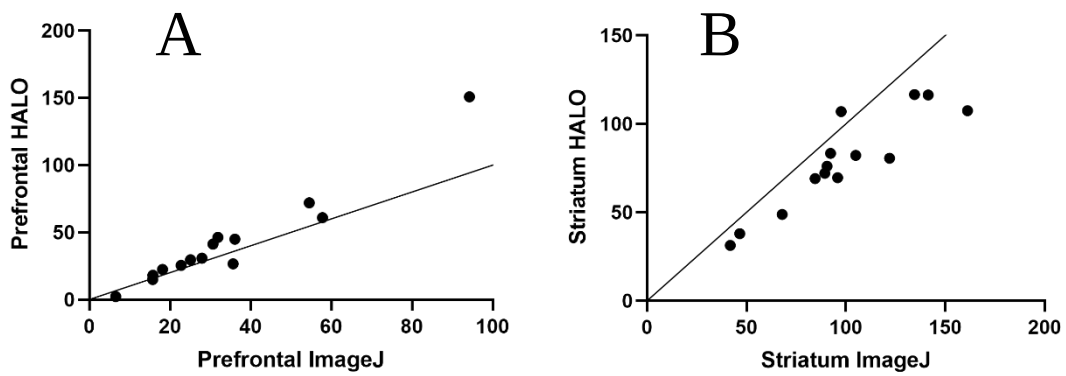

Figure 4: Correlation between counts on ImageJ and HALO. Microglia number per mm² were quantitated as described in figure 3 in ImageJ and by an independent assessor in HALO. Results were subjected to Pearson's correlation analysis. a) PFC correlation, p<0.0001, r=0.96. b) Striatum correlation, p<0.0001, r=0.90.

3.2 Microglial activation analysis in control and PD

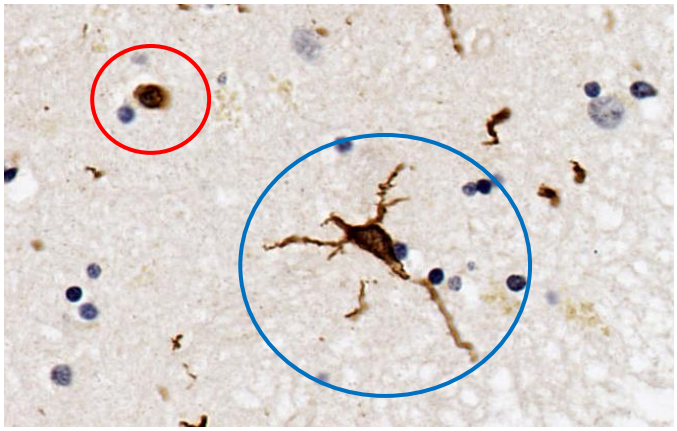

Figure 6: Activated (red) vs Non-activated microglia (blue). ImageJ circularity parameters were used to determine microglia activation state.

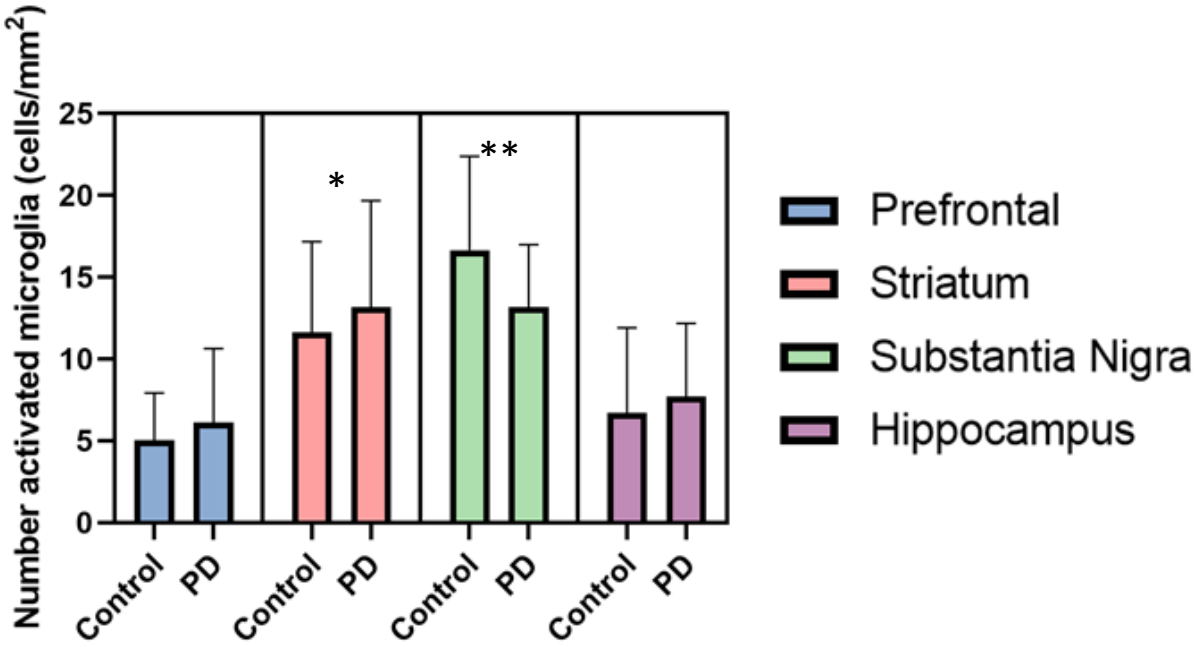

*Figure 5: Activated microglia per mm² in control vs PD cohort. Cells were quantitated in ImageJ n=11 PD, n=5 control. Data was analysed by two-way ANOVA. No significant differences were observed between control and PD within each region. */** = significantly different to other regions*

There was a significant main effect of region as shown in figure 5 ($F(3,36) = 22.68$, $p < 0.0001$). The number of activated microglia in the SN (14.92 (1.27)), were significantly higher than in the striatum (11.17 (1.11), $p < 0.05$), PFC (4.82 (0.81), $p < 0.001$) or hippocampus (7.02 (1.37), $p < 0.001$). Similarly, the number of activated microglia in the striatum were elevated compared to the PFC ($p < 0.001$) or hippocampus ($p < 0.01$), although these regions did not differ from one another ($p = 0.103$). Regarding group, activated microglia were not significantly different in PD (8.97

(0.98)) compared to healthy controls (10.00 (1.32); F (1, 12) = 0.396, p = 0.541). There was no significant interaction between region and group (F (3, 36) = 0.878, p = 0.445).

Activation analysis was performed on HALO independently of ImageJ counting (appendix d). Correlational analysis between counts were performed in the PFC (p=0.0024, r=0.74) (Figure 6a) and striatum (p=0.0134, r=0.64) (Figure 6b) where significant correlations were observed.

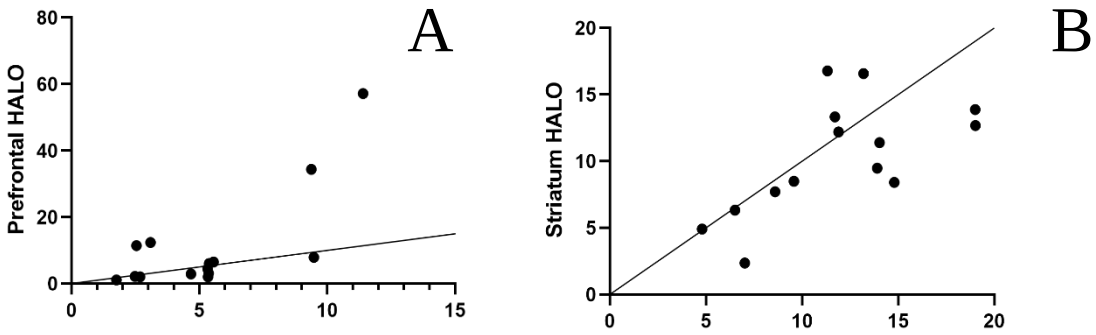

Figure 6: Correlation between activated microglia counts on ImageJ and HALO. Microglia number per mm² were quantitated as described in figure 3 in ImageJ and by an independent assessor in HALO. Results were subjected to Pearson's correlation analysis. a) PFC correlation, p=0.0024, r=0.74. b) Striatum correlation, p=0.0134, r=0.64.

3.3 BV-2 cell viability assessed using MTT assay

Following treatment with NPs, MTT assays were performed assessing viability of BV-2 cells. Figure 7a shows the viability of BV-2 cells following incubation with GNPs alone. No significant differences were observed between the control and the treatments at any dose however the viability differed significantly between timepoints for 3µg/mL (2 vs 24hrs, p=0.03). Co-treatment with LPS alongside NPs, (figure 7b) did not significantly differ from control ($F(1, 125)=1.06$, $p=0.38$) however there was a decrease overtime at 300µg/mL (2 vs 48hrs, p=0.04) ($F(1,125)=3.48$, $p=0.03$).

Viability of BV-2 cells after incubation with CNTs are shown in figure 7c. At 2hrs, viability was significantly lower than control for treatments of 30 (p=<0.0001) and 300µg/mL (p=<0.0001). CNTs at 300µg/mL (24hr-p=<0.0001, 48hr-p=0.003) remained significantly lower than control at

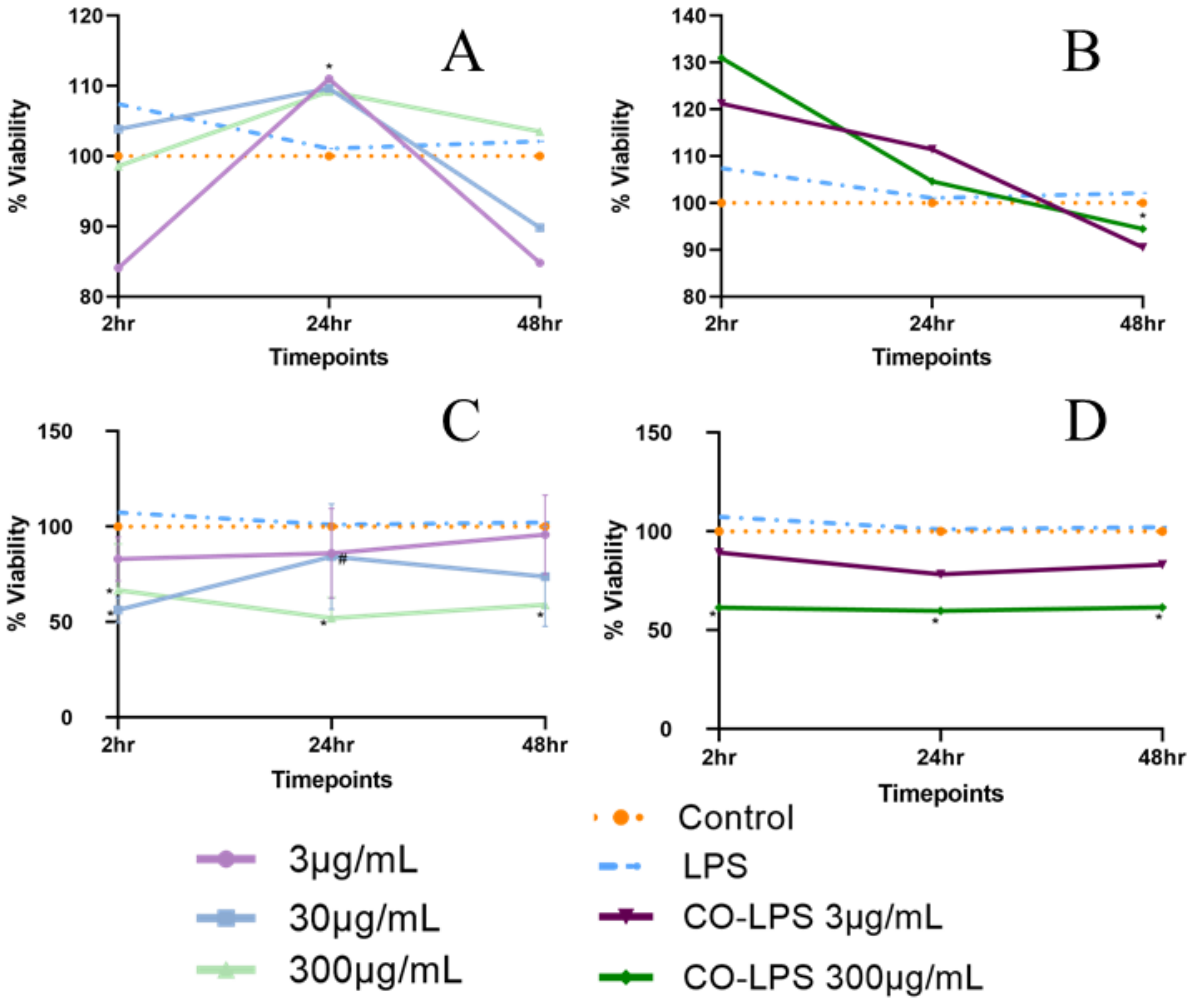

*Figure 7: BV2 viability after treatment with a) GNPs, b) GNPs+LPS, c) CNTs, d) CNTs+LPS. Cell viability was assessed using MTT assays and results analysed using a two-way ANOVA. No significant differences were observed between doses. * = significant difference from 2-hour timepoint p=<0.05.*

both 24- and 48hr timepoints. Comparisons between timepoints showed a significant increase in viability for CNT at 30µg/mL (24hrs, p=0.01). Co-treatment with CNTs+LPS (figure 7d) at 300µg/mL (p=0.005) (F (6,125) =17.49, p=<0.0001) significantly lowered cell viability at all timepoints (24hr-p=0.001, 48hr-p=0.007).

3.5 BV-2 IL-6 release assessed using ELISA

Supernatants were analysed using ELISAs for release of IL-6 by BV-2 cells. Figure 8a/b shows IL-6 release after administration of GNPs with significant effect for time (F (2,117) = 46.41, p<0.0001) and treatment (F (6,117) = 40.65, p<0.0001). There was no observed effect of GNPs alone (p=0.9977 at any timepoint) but LPS control differed significantly from the vehicle control after 24 (p=0.02) and 48hrs (p<0.0001). For cells co-treated with GNPs and LPS, IL-6 release was

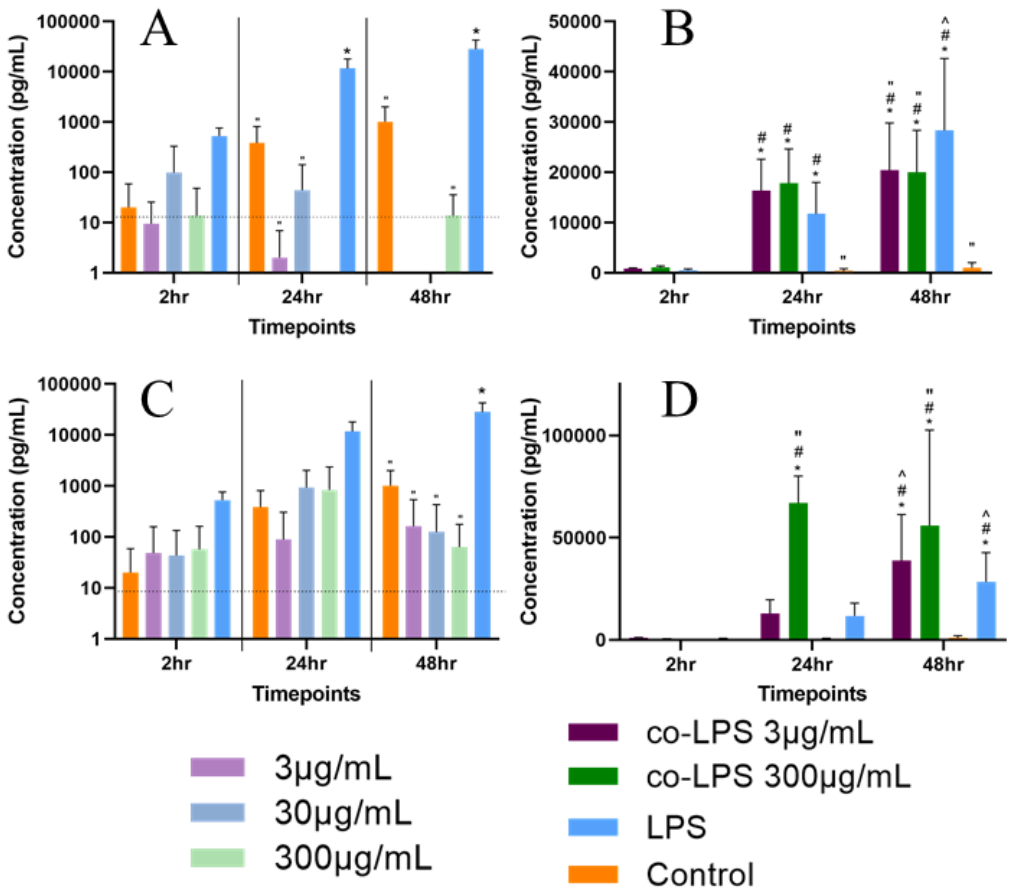

*Figure 8: IL-6 release from BV2 cells following treatment with a) GNPs, b) GNP+LPS, c) CNTs, d) CNTs+LPS. ELISAs were used to quantify IL-6 release and results were analysed using 2 two-way ANOVAs. * = significant difference from vehicle control at relative timepoint, # = significant difference from the relative dose at 2hr timepoint, ^ = significant difference from relative dose at 24hr timepoint, " = significant difference from LPS control at relative timepoint.*

significantly higher for both 3µg/mL (24hr-$p<0.0001$, 48hr-$p<0.0001$) and 300µg/mL (24hr-$p<0.0001$, 48hr-$p<0.0001$) compared to the 2hr timepoint.

Figure 8c/d shows IL-6 release by BV-2 cells after CNTs with significant effect for time ($F(2,117) = 24.92$, $p<0.0001$) and treatment ($F(6,117) = 26.35$, $p<0.0001$). There was no effect of CNTs alone ($p>0.99$ at any timepoint) but LPS control differed significantly from the vehicle control at 48hrs ($p=0.0005$). For cells co-treated with CNTs and LPS, IL-6 release was significantly higher for both 3µg/mL (48hr-$p<0.0001$) and 300µg/mL (24hr-$p<0.0001$, 48hr-$p<0.0001$) compared to the vehicle control. Over time IL-6 release was significantly higher for both 3µg/mL (48hr-$p<0.0001$) and 300µg/mL (24hr-$p<0.0001$, 48hr-$p<0.0001$) compared to the 2hr timepoint.

4. Discussion

Understanding the CNS immune response is key in developing treatments for NDs. The role of microglia in neuroinflammation highlights the need to investigate this cell type. This research aimed to quantify microglia and assess microglial activation within key brain regions in a PD cohort and investigate the response of microglia-like cells *in vitro* to administration of GNPs and CNTs as potential therapeutics for PD treatment.

Analysis of human tissue stained for IBA1, a marker of microglia, revealed no differences in total number or number of activated microglia between control and PD cohorts. Numbers of total and activated microglia were increased in the SN> striatum with both regions significantly higher than the PFC and hippocampus. These findings highlight the striatum and SN as regions of the brain most relevant to microglial function and likely regions of the brain to focus on in future studies.

While our study found no differences between control and PD microglia, other studies in post-mortem human tissue found increases in activated microglia in the SN and hippocampus, and in the putamen, a specific region of the striatum[43, 44]. These differences were shown via detection of elevated levels of major histocompatibility complex (MHC) class II expressing-cells, which is a marker present on mononuclear phagocytes such as microglia[43]. Additionally, microglia clustering around dopaminergic neurons in the SN in patients with 1-methyl-4-phenyl-1,2,3,6-tetrahydropyridine (MPTP) induced Parkinsonism, up to 16 years after exposure to the toxin, is reported[45].

Methodological differences in these studies when compared to the current study may explain some of the difference in results. Imamura et al,[43] employed a similar cohort number to ours (12 PD cases and 4 controls) however, the cohort was more homogenous, with age-matched cases and well defined criteria within groups. In terms of staining and counting methods, standard IHC methods were used but markers differed between studies, for instance IBA1 used here, and MHC-II, and CD11a/b staining used by others, which may be superior in differentiating activated from inactivated microglia[12, 43]. Other methods quantified microglial presence and function by analysis of

inflammatory cytokines, such as TNF-α [43, 45, 46]. In most prior publications the exact methods used to count cells are unstated but are thus likely to be manual counting. In the present study, two automated methods were used and should be compared to manual counting.

A notable limitation of the quantitation of microglia is the activation analysis on ImageJ, where only circularity is used as a parameter of activation. Similarly, in a prior study 'amoeboid' (round) microglia were enumerated and demonstrated to be increased in PD brain[44]. However, this is simplistic and when analysing microglial activation states, whole cell morphology should be considered, including process thickness, length, and cell circularity[47]. HALO microglial activation analysis, which was used to verify counts on ImageJ, takes these factors into account; however, there are no previously verified ranges for these parameters and thus the method is still in the optimisation stage.

The results seen in here may also reflect the stage of PD assessed, where post-mortem human tissue limits analysis to late stage PD. Although the study of MPTP induced parkinsonism suggests that microglial presence at damaged sites persist beyond neuronal cell death[45], there may not be as significant numbers of microglia present late in disease compared to the early stage neuronal death[12]. IBA1, the marker used to identify microglia in the present study, is a marker specific to macrophages as well as microglia, and is normally discriminate in brain tissue as peripheral macrophages are not present. However, in the case of late stage PD where there is breakdown of the BBB and infiltration of peripheral macrophages, IBA1 may not be as accurate at specifically detecting microglia, and potentially the levels of microglia seen in control tissue maybe the result of infiltration of peripheral macrophages prior to death in this cohort. As well as the issue of peripheral macrophages, IBA1 does not discriminate between active and inactive microglia. Using a marker of activated microglia such as CD68[48], which is expressed at high levels by activated microglia, may be of better use in further investigations into activation states or such as in studies above, CD11b/a and CD54[12, 43] may be employed as an alternative marker of microglia. Alternatively, analysis could be further refined to assess variation in distribution of microglia between different regions of the brain.

In the second aim of our study, the pathological environment in PD was mimicked *in vitro* by stimulating a mouse microglia-like cell line (BV-2) with inflammation-inducing LPS. In this setting, we assessed the neurotoxic effects of GNPs and CNTs, with the pretext that these nanoparticles can be potentially used as diagnostic probes or drug delivery vehicles for the brain-targeted treatment of PD. GNPs have the potential to be used in both PD treatment, for therapeutic delivery, and as a contrast agent in diagnostic brain imaging[29, 49]. Both applications require an understanding of the effects and safety of GNPs in brain specific environments. When administered alone, GNPs showed no effect on BV-2 viability or the induction of the pro-inflammatory cytokine IL-6. However, when administered in conjunction with LPS, GNPs decreased cellular viability at 300µg/mL (1.6-fold) and 3µg/mL (1.3-fold) at 24 and 48hr respectively in comparison to LPS alone. IL-6 release was also reduced at both 3 and 300µg/mL at the 48hr compared to LPS control. These results indicate that GNPs alone are not toxic and do not induce inflammation in BV-2 cells. However, in a pre-existing inflammatory environment induced by LPS, GNPs decreased cell viability but reduced the inflammatory response in a dose and time-dependent manner. While decreased cell viability is an unwanted effect, decreased inflammatory response may be beneficial if GNPs are to be used in therapeutic interventions where inflammation is linked to pathology. It remains to be determined if the observed decrease in IL-6 is due to reduced viability and cell number, which may impact the capacity of cells to make IL-6. As discussed above, GNPs when loaded with the antioxidant anthocyanin, increased the drugs anti-inflammatory effects[30]. Whether these effects are a result of delivering more of the drug to the site or due to possible anti-inflammatory effects of the GNPs themselves remains to be understood. In another instance, GNPs functionalised with deoxyrubozyme (DNAzyme) were observed to have anti-inflammatory effects on TNF-α secretion in a rat model of myocardial infarction, further promoting inquiry into the anti-inflammatory effects of GNPs[50]. Thus further investigation is required to determine any beneficial effects GNPs have on IL-6 production by microglia. This may include testing at different doses and longer incubation times, as well as other GNPs with varying physicochemical properties (e.g. size, shape, surface charge) such as nanorods or

nanocubes[51]. The GNPs used in this study were chosen due to their widespread use in the scientific literature and commercial availability.

CNTs are of interest for PD treatment as they may be tolerated when coated with biocompatible polymers [52]. In our study when CNTs were administered alone, there was a significantly decrease in BV-2 viability compared to vehicle control at high doses (300µg/mL) at all three time-points tested. After 2hr, viability decreased for the 30µg/mL dose, but this effect was not seen at later time-points, which could indicate an acute stress response from cells upon the addition of CNTs, with cell recovering after longer incubation. No cytotoxicity was observed for 3µg/ml of CNTs, therefore high but not lower doses appear to be toxic. In contrast to the observed cytotoxicity of CNTs, there was no increase in IL-6 release compared to the vehicle control, indicating no induction of inflammation. Similar to when administered alone, CNTs at 300µg/mL in combination with LPS significantly decreased viability at all timepoints. IL-6 release for LPS+CNT co-treatments at 300µg/mL was significantly higher than the LPS alone at 24 and 48 hours. CNT at 3µg/ml did not affect the LPS-induction of IL-6 or cell viability at any time point. This demonstrates that CNTs alone do not induce any significant inflammatory responses in BV-2 cells but do worsen their LPS-induced inflammatory response. Additionally, CNT at high doses had a significant impact on the viability of cells both in pro-inflammatory and non-inflammatory environments. This suggests that care must be taken in the administered dose that can be tolerated for future therapy. Using light microscopy, CNTs were observed to readily precipitate and accumulate on the surface of cells, which may contribute to cytotoxic effect. This cytotoxicity was previously observed by Davoren et al., 2007, wherein single walled CNTs (SWCNTs), as used in the present study, formed visible aggregates at 800µg/mL on A549 lung cancer cells in culture, [53]. This aggregation was seen after 24hrs whereas in our study, aggregated CNTs were observed immediately after administration. This may be due to the different intensities of sonication methods used, here an ultrasonic bath was used and a stick sonicator used by Davoren et al[53]. Alternatively, the CNT's may have interfered with the MTT assay, as has been previously documented[54]. A substitute to this assay may be used such as WST-1, an alternative

tetrazolium salt[54]. Comparative studies on multi-walled CNTs (MWCNT) suggest they do not show as much toxicity as SWCNTs and therefore may be an alternative for testing in the future. Further, the mechanism by which CNTs induce toxicity should be investigated. Potential pathways include recognition as danger signals by engaging innate immune receptors such as toll-like receptors (TLRs)[55] that can be assessed via analysis of downstream signalling pathways or using TLR antagonists.

Based on our findings, GNPs exhibited a broader safety profile and less potential toxicity via inflammatory routes than CNTs and would therefore be more suitable as therapeutic tools for PD. This data also informs understanding about the effects of NP shape on toxicity, as the tube shape of the CNTs may be compared to the spherical GNPs used here. While these factors were not extensively analysed in this study, there is evidence for the asbestos-like shape of CNTs contributing to increased toxicity[34, 56], further supporting GNPs as preferable to CNTs in PD treatment.

It is of note, however, that there was large variability in the results presented here and future work should include more experimental replicates. Additionally, this data forms a foundation to assess NPs in terms of dose range and with cells pre-treated, rather than co-treated, with other inflammatory stimuli, such as PAMcsk or TNF-α. Further, assessment of the release of other inflammatory markers such as TNF-α or nitric oxide, both of which have been implicated in PD pathology may be of future interest [39]. Additionally, as the CNS environment changes with age, a model of aged cells in culture is of interest for further investigation[9].

Overall, this study has shown that in post-mortem human PD tissue microglial numbers are not increased and suggests GNP's should be studied further as potential therapeutic delivery vehicles for PD. This data lays a foundation for further study of microglia in the PD brain and the utility of NPs in treatment of neurological diseases.

Professional & funding acknowledgements

Funding for this research was provided by The Brain Foundation, The NeuroSurgical Research Foundation and Dementia Australia. Along with support from the ARC Centre of Excellence: Centre for Nanoscale BioPhotonics.

References

1. Gautam, R. and M. Sharma (2020) Prevalence and Diagnosis of Neurological Disorders Using Different Deep Learning Techniques: A Meta-Analysis. Journal of Medical Systems. **44**. 1-24.
2. Whiteford, H.A., et al. (2015) The Global Burden of Mental, Neurological and Substance Use Disorders: An Analysis from the Global Burden of Disease Study 2010.(Research Article). PLoS ONE. **10**. e0116820.
3. Feigin, V.L., et al. (2019) Global, regional, and national burden of neurological disorders, 1990–2016: a systematic analysis for the Global Burden of Disease Study 2016. The Lancet Neurology. **18**. 459-480.
4. Gitler, A.D., P. Dhillon, and J. Shorter (2017) Neurodegenerative disease: models, mechanisms, and a new hope. Disease Models & Mechanisms. **10**. 499-502.
5. Scialò, C. and G. Legname (2020) How would defining Parkinson's as a prion disease impact the search of a cure? Expert Review of Neurotherapeutics. **20**. 417-420.
6. Cragnolini, A., et al. (2020) Regional brain susceptibility to neurodegeneration: what is the role of glial cells? Neural Regeneration Research. **15**. 838-842.
7. Iarkov, A., et al. (2020) Strategies for the Treatment of Parkinson's Disease: Beyond Dopamine. Frontiers in Aging Neuroscience.
8. Barker, R.A., et al. (2019) Designing stem-cell-based dopamine cell replacement trials for Parkinson's disease. Nature Medicine. **25**. 1045-1053.
9. Suescun, J., S. Chandra, and M.C. Schiess (2019), *Chapter 13 - The Role of Neuroinflammation in Neurodegenerative Disorders*, in *Translational Inflammation*, J.K. Actor and K.C. Smith, Editors, Academic Press. p. 241-267.
10. Niranjan, R. (2018) Recent advances in the mechanisms of neuroinflammation and their roles in neurodegeneration. Neurochemistry International. **120**. 13-20.
11. Wee Yong, V., *Inflammation in Neurological Disorders: A Help or a Hindrance?* 2010, SAGE Publications: Los Angeles, CA. p. 408-420.
12. McGeer, P.L. and E.G. McGeer (2008) Glial reactions in Parkinson's disease. Movement Disorders. **23**. 474-483.
13. Teismann, P. and J.B. Schulz (2004) Cellular pathology of Parkinson's disease: astrocytes, microglia and inflammation. Cell and Tissue Research. **318**. 149-161.
14. Kim, Y.S. and T.H. Joh (2006) Microglia, major player in the brain inflammation: their roles in the pathogenesis of Parkinson's disease. Experimental & Molecular Medicine. **38**. 333-347.
15. Bachiller, S., et al. (2018) Microglia in Neurological Diseases: A Road Map to Brain-Disease Dependent-Inflammatory Response. Frontiers in Cellular Neuroscience. **12**. 488.
16. McGeer, P.L., et al. (1988) Reactive microglia are positive for HLA-DR in the substantia nigra of Parkinson's and Alzheimer's disease brains. Neurology.
17. Furtado, D., et al. (2018) Overcoming the Blood-Brain Barrier: The Role of Nanomaterials in Treating Neurological Diseases. Advanced materials (Deerfield Beach, Fla.). **30**. e1801362.
18. Reichel, A. (2009) Addressing Central Nervous System (CNS) Penetration in Drug Discovery: Basics and Implications of the Evolving New Concept. Chemistry & Biodiversity. **6**. 2030-2049.
19. Daniel Mihai, T., et al. (2018) Impact of Nanoparticles on Brain Health: An Up to Date Overview. Journal of clinical medicine. **7**. 490.

20. Mary Ealias, A. and S. M P (2017) A review on the classification, characterisation, synthesis of nanoparticles and their application. IOP Conference Series Materials Science and Engineering. **263**. 032019.
21. Singh, A.K. (2016), *Chapter 1 - Introduction to Nanoparticles and Nanotoxicology*, in *Engineered Nanoparticles*, A.K. Singh, Editor, Academic Press: Boston. p. 1-18.
22. Lee, E.J., N.K. Lee, and I.-S. Kim (2016) Bioengineered protein-based nanocage for drug delivery. Advanced Drug Delivery Reviews. **106**. 157-171.
23. Zhou, Y., et al. (2018) Crossing the blood-brain barrier with nanoparticles. Journal of Controlled Release. **270**. 290-303.
24. Cook, R.L., et al. (2015) A critical evaluation of drug delivery from ligand modified nanoparticles: Confounding small molecule distribution and efficacy in the central nervous system. Journal of controlled release. **220**. 89-97.
25. Bardi, G., et al. (2013) Functionalized Carbon Nanotubes in the Brain: Cellular Internalization and Neuroinflammatory Responses. PloS one. **8**. e80964.
26. Sridhar, V., et al. (2018) Pharmacokinetics and pharmacodynamics of intranasally administered selegiline nanoparticles with improved brain delivery in Parkinson's disease. Nanomedicine: Nanotechnology, Biology and Medicine. **14**. 2609-2618.
27. Carradori, D., et al. (2018) Antibody-functionalized polymer nanoparticle leading to memory recovery in Alzheimer's disease-like transgenic mouse model. Nanomedicine: Nanotechnology, Biology and Medicine. **14**. 609-618.
28. Balasubramanian, S.K., et al. (2013) The effect of primary particle size on biodistribution of inhaled gold nano-agglomerates. Biomaterials. **34**. 5439-5452.
29. Flora, S.J.S. (2017), *Chapter 8 - The Applications, Neurotoxicity, and Related Mechanism of Gold Nanoparticles*. Elsevier Inc. 179-203.
30. Kim, M.J., et al. (2017) Enhanced neuroprotection of anthocyanin-loaded PEG-gold nanoparticles against Aβ1-42-induced neuroinflammation and neurodegeneration via the NF-KB /JNK/GSK3β signaling pathway. Nanomedicine: Nanotechnology, Biology and Medicine. **13**. 2533-2544.
31. Zhang, X.-D., et al. (2012) In vivo renal clearance, biodistribution, toxicity of gold nanoclusters. Biomaterials. **33**. 4628-4638.
32. Patra, H.K., et al. (2007) Cell selective response to gold nanoparticles. Nanomedicine: Nanotechnology, Biology and Medicine. **3**. 111-119.
33. Hu, H., et al. (2004) Chemically Functionalized Carbon Nanotubes as Substrates for Neuronal Growth. Nano letters. **4**. 507-511.
34. Shi, D., G. Mi, and T.J. Webster (2017), *Chapter 11 - The Synthesis, Application, and Related Neurotoxicity of Carbon Nanotubes*, in *Neurotoxicity of Nanomaterials and Nanomedicine*, X. Jiang and H. Gao, Editors, Academic Press. p. 259-284.
35. Sato, Y., et al. (2005) Influence of length on cytotoxicity of multi-walled carbon nanotubes against human acute monocytic leukemia cell line THP-1 in vitro and subcutaneous tissue of rats in vivo. Molecular BioSystems. **1**. 176-182.
36. Liu, Z., et al. (2008) Drug Delivery with Carbon Nanotubes for In vivo Cancer Treatment. Cancer research (Chicago, Ill.). **68**. 6652-6660.
37. Yang, F., et al. (2011) Magnetic functionalised carbon nanotubes as drug vehicles for cancer lymph node metastasis treatment. European Journal of Cancer. **47**. 1873-1882.
38. Foldbjerg, R., et al. (2014) The toxic effects of single-walled carbon nanotubes are linked to the phagocytic ability of cells. Toxicology research (Cambridge). **3**. 228.
39. Hirsch, E.C., S. Vyas, and S. Hunot (2012) Neuroinflammation in Parkinson's disease. Parkinsonism & Related Disorders. **18**. S210-S212.
40. Bankhead, P., et al. (2017) QuPath: Open source software for digital pathology image analysis. Scientific Reports. **7**. 16878.
41. Schneider, C.A., W.S. Rasband, and K.W. Eliceiri (2012) NIH Image to ImageJ: 25 years of image analysis. Nature Methods. **9**. 671-675.

42. Varghese, F., et al. *IHC Profiler: An Open Source Plugin for the Quantitative Evaluation and Automated Scoring of Immunohistochemistry Images of Human Tissue Samples (Open Source Plugin for IHC Image Scoring)*. 2014. **9**, e96801 DOI: 10.1371/journal.pone.0096801.
43. Imamura, K., et al. (2003) Distribution of major histocompatibility complex class II-positive microglia and cytokine profile of Parkinson's disease brains. Acta Neuropathologica. **106**. 518-526.
44. Knott, C., et al. (2002) Elevated glial brain-derived neurotrophic factor in Parkinson's diseased nigra. Parkinsonism & Related Disorders. **8**. 329-341.
45. Langston, J.W., et al. (1999) Evidence of active nerve cell degeneration in the substantia nigra of humans years after 1-methyl-4-phenyl-1,2,3,6-tetrahydropyridine exposure. Annals of neurology. **46**. 598-605.
46. Jyothi, H.J., et al. (2015) Aging causes morphological alterations in astrocytes and microglia in human substantia nigra pars compacta. Neurobiology of Aging. **36**. 3321-3333.
47. Nimmerjahn, A. (2005) Resting Microglial Cells Are Highly Dynamic Surveillants of Brain Parenchyma in Vivo. Science (American Association for the Advancement of Science). **308**. 1314-1318.
48. Joers, V., et al. (2017) Microglial phenotypes in Parkinson's disease and animal models of the disease. Progress in neurobiology. **155**. 57-75.
49. Gonzalez-Carter, D.A., et al. (2019) L-DOPA functionalized, multi-branched gold nanoparticles as brain-targeted nano-vehicles. Nanomedicine: Nanotechnology, Biology and Medicine. **15**. 1-11.
50. Somasuntharam, I., et al. (2016) Knockdown of TNF-α by DNAzyme gold nanoparticles as an anti-inflammatory therapy for myocardial infarction. Biomaterials. **83**. 12-22.
51. Elahi, N., M. Kamali, and M.H. Baghersad (2018) Recent biomedical applications of gold nanoparticles: A review. Talanta (Oxford). **184**. 537-556.
52. Tan, J.M., et al. (2018) Incorporation of Levodopa into Biopolymer Coatings Based on Carboxylated Carbon Nanotubes for pH-Dependent Sustained Release Drug Delivery. Nanomaterials (Basel, Switzerland). **8**. 389.
53. Davoren, M., et al. (2007) In vitro toxicity evaluation of single walled carbon nanotubes on human A549 lung cells. Toxicology in Vitro. **21**. 438-448.
54. Wörle-Knirsch, J.M., K. Pulskamp, and H.F. Krug (2006) Oops They Did It Again! Carbon Nanotubes Hoax Scientists in Viability Assays. Nano Letters. **6**. 1261-1268.
55. Pallardy, M.J., I. Turbica, and A. Biola-Vidamment (2017) Why the Immune System Should Be Concerned by Nanomaterials? Frontiers in immunology. **8**. 544-544.
56. Park, E.-J., et al. (2011) Biological Toxicity and Inflammatory Response of Semi-Single-Walled Carbon Nanotubes. PLOS ONE. **6**. e25892.

Appendix A

Clinical case details control patient

Australian Brain Bank Network SA0162
South Australian Brain Bank Control
Clinical Case Details

Case No: SA0162 **Sex:** M **Age:** 72 yrs **PMI:** 30 hrs

Cause of death: Methicillin-resistant staphylococcus aureus (MRSA)

Background information: No known neurological disease. Duane's syndrome (eyes), dyslexic but completed engineering degree and degree in theoretical physics. Colourblind. Hypoxic episodes over last few months of life. High blood pressure, heart disease. Aortic stenosis, cirrhosis of liver, hypertension, ischaemic heart disease, paroxysmal atrial fibrillation, recurrent GI bleeds,

Medication History: Lipitor, Inderal, Thiamine, Spironalactone, Amiodorone, Ventolin, Lasix, Losec, Nitrolingual spray, Pneumococcal vaccine, influenza vaccine, tetanus toxoid vaccine, fluvax, Lanoxin, Propranolol.

Diagnosis: Normal - Control (brain and spinal cord)

MICROSCOPIC BRAIN REPORT:

Right hemi-midbrain (N1-N3): Mild patchy loss of pigmented neurons of the substantia nigra with pigmentary incontinence and mild reactive gliosis. No Lewy bodies. Mild fibrous gliosis of periaqueductal grey matter.

Rostral pons (N4,N5,N6,N7,N8): Normal for age. Occasional pigmentary incontinence of locus coeruleus neurons. No Lewy bodies.

Pons at level of abducens and facial nuclei (N9,N10): The facial nucleus is normal. Moderate loss of abducens' neurons with little evidence of reactive change.

Right hemi-medulla (N11,N12,N13,N14): Prominent neuroaxonal spheroids in gracile and cuneate nuclei consistent with age.

Right vermis (N15): Normal for age.

Right cerebellar hemisphere (N16): Normal for age.

Right superior, middle and inferior frontal gyri (N17,N18,N19): Normal for age. The Bielschowsky silver stains show no plaques or tangles.

Right cingulate gyrus (N20): Normal. The Bielschowsky silver stain shows no plaques or tangles.

Right basal ganglia (N21): Normal for age including Bielschowsky silver stain.

Right basal ganglia and thalamus (N22): Mild status cribrosus of putamen. Otherwise normal.

Right amygdaloid nuclei (N23): Normal. The Bielschowsky silver stain shows no plaques or tangles.

South Australian Brain Bank
In collaboration with the Australian Brain Bank Network
Flinders University, Department of Human Physiology, Sturt Road, Bedford Park SA 5042, Australia
IMVS

South Australian Brain Bank
Clinical Case Details ... continued

Right thalamus (N24): Normal including a subthalamic nucleus. The Bielschowsky silver stain shows no plaques or tangles.

Right temporal lobe (N25) and right hippocampus (N26): Normal including Bielschowsky silver stains. Only the very occasional isolated senile plaque is present.

Right inferior parietal lobule (N27): Normal including Bielschowsky silver stain. No senile plaques or tangles.

Right superior parietal cortex (N28): Normal including Bielschowsky silver stain.

Corpus callosum (N29): Patchy congestion.

Right calcarine cortex (N30): Normal for age. The Bielschowsky silver stain shows no senile plaques or neurofibrillary tangles.

C2-coccygeal 1 and phylum terminale (N31-N61): The H & E and Weil stains are normal for age.

CONCLUSION:
Normal brain and spinal cord for age.

PROFESSOR P C BLUMBERGS

Appendix B

Australian Brain Bank Network

South Australian Brain Bank

SA0127
PD

Clinical Case Details

Case No: SA0127 **Sex:** M **Age:** 74 yrs **PMI:** 3 1/2 hrs

Cause of death: End stage Parkinson's disease, dysphagia secondary to PD. Died 2003.

Background information: 15 year history of Parkinson's disease. Neuro 1992: First noticed left leg tremor in 1989. Good results on madopar and remained quite well since. Last 6 months intermittent tremor in left upper limb. Remains independent. Some weight loss early but stabilised. Left hemiparkinsonism characterized mainly by tremor. Functional disability minimal though some end-of-dose loss of effect. 1995: Developed increasing tremor greater on the right side. Feels a little slow at night. Tremor in all four limbs made worse by anxiety. Rigidity and bradykinesia were mild. Walked freely with no arm swing. Some difficulty getting in and out of bed and turning in bed. 1998 Pergolide beneficial. Increasing bouts of freezing but still quite mobile and independent. One fall. Persistent rhythmic tremor of the upper limbs, moderate rigidity and bradykinesia. Walking freely. 2002 Pneumonia (right middle lobe) and urinary tract infection. Occasional difficulty in swallowing associated with PD. Gastro-oesophageal reflux. Hiatus hernia. Palliative care for last 2 weeks of life.
Medication included: Sinemet, Pantoprazole, Paracetamol, Madopar, Morphine, Pergolide

Diagnosis: Lewy body Parkinson's disease (idiopathic Parkinson's disease)

MICROSCOPIC BRAIN REPORT:
Right hemi-midbrain (N1): Severe neuronal loss of pigmented neurons from the substantia nigra, pigmentary incontinence and intracytoplasmic Lewy bodies and pale bodies in some of the residual nerve cells. Neuronal loss and gliosis in the pars reticularis. The alpha-synuclein immunostain shows immunopositive Lewy body neurites, cytoplasmic immunoreactivity in some of the residual nerve cells and immunopositive Lewy bodies.

Pons (N2,N3,N4,N5,N6,N7,N8): Severe loss of pigmented neurons from locus coeruleus. Many residual nerve cells show single or multiple intracytoplasmic Lewy bodies. The alpha-synuclein immunostains show Lewy body neurites, intracytoplasmic immunostaining and immunopositive Lewy bodies. Midline raphe neurons show similar spectrum of alpha synuclein abnormalities.

Medulla (N9,N10,N11,N12,N13,N14): The alpha synuclein immunostains show immunopositive Lewy bodies, Lewy body neurites and intracytoplasmic staining of nerve cells of the dorsomotor vagal nucleus. Similar alpha-synuclein abnormalities are present in some of the reticular formation nerve cells and in the midline raphe.

Right cingulate gyrus (N17): The alpha-synuclein immunostain shows very occasional cortical Lewy bodies involving pyramidal cells of the deeper cortical layer. The Bielschowsky silver stain shows no evidence of senile plaques or neurofibrillary tangles.

Right superior frontal gyrus (N16): The alpha-synuclein immunostain shows only very occasional cortical Lewy bodies. The Bielschowsky silver stain is negative for senile plaques and neurofibrillary tangles.

South Australian Brain Bank
In collaboration with the Australian Brain Bank Network
Flinders University, Department of Human Physiology, Sturt Road, Bedford Park SA 5042, Australia

Director:
Professor Peter
Division of Neuropathology
Institute of Medical and Veterinary Science

Professor Bill Blessing
Neurology Department
Flinders University/Flinders Medical Centre

Coordinator:
Ms Robyn
Department of Human Physiology
Flinders University
Sturt Road
Bedford Park SA 5042
Australia

IMVS

South Australian Brain Bank
Clinical Case Details ... continued

Right middle frontal gyrus (N19) and right inferior frontal gyrus (N20): The alpha-synuclein immunostains are negative. The Bielschowsky silver stains show no evidence of plaques or tangles.

Right hippocampus (N21): The Bielschowsky silver stain shows some scattered neurofibrillary tangles restricted to the entorhinal cortex. The pyramidal cells of Ammon's horn are not involved. There is no senile plaque formation. Very occasional deep cortical neurons show alpha-synuclein immunopositive cytoplasmic inclusions.

Right basal ganglia (N18,N22): Very occasional deep cortical insular neurons show alpha-synuclein immunopositive cytoplasmic inclusions. Prominent alpha-synuclein immunopositive myelinated fibres (tram-lines') are noted in the globus pallidus.

Right thalamus (N23): Normal for age.

Right parietal cortex (N24) and right calcarine cortex (N25): Very occasional alpha-synuclein immunopositive cytoplasmic inclusions in the deep cortical nerve cells of the parietal cortex. The Bielschowsky silver stains show no plaques or tangles.

CONCLUSION:
The features are those of Lewy body Parkinson's disease (idiopathic Parkinson's disease).

PROFESSOR P C BLUMBERGS

Appendix C

Heat maps of total microglia counts in prefrontal and striatum ImageJ vs HALO

Prefrontal ImageJ					PD								Controls			
	SA0051	SA0062	SA0067	SA0076	SA0086	SA0103	SA0127	SA0131	SA0230	SA0250	SA0277	SA0021	SA0031	SA0096	SA0162	SA0214
Cells per mm^2	57.81	27.94	15.72	25.07	15.76	22.73	78.5	36.09	94.25	8.7	18.16	30.64	35.62	6.55	31.86	54.5
Prefrontal HALO																
	SA0051	SA0062	SA0067	SA0076	SA0086	SA0103	SA0127	SA0131	SA0230	SA0250	SA0277	SA0021	SA0031	SA0096	SA0162	SA0214
Cells per mm^2	60.87	30.82	14.9	29.63	18.1	25.46		44.93	150.72		22.37	41.21	26.51	2.33	46.3	71.99

Striatum ImageJ					PD								Controls			
	SA0051	SA0062	SA0067	SA0076	SA0086	SA0103	SA0127	SA0131	SA0230	SA0250	SA0277	SA0021	SA0031	SA0096	SA0162	SA0214
Cells per mm^2	162.32	89.4	97.56	92.27	46.64	90.52	104.91	161.13	134.53	41.78	84.49	95.83	141.43	36.06	67.99	121.92
Striatum HALO																
	SA0051	SA0062	SA0067	SA0076	SA0086	SA0103	SA0127	SA0131	SA0230	SA0250	SA0277	SA0021	SA0031	SA0096	SA0162	SA0214
Cells per mm^2		72.04	106.91	83.35	37.94	76.1	82.14	107.49	116.55	31.28	69.04	69.53	116.36		48.85	80.56

Appendix D

Heat maps of activation analysis in prefrontal and striatum ImageJ vs HALO

Prefrontal ImageJ					PD								Controls			
	SA0051	SA0062	SA0067	SA0076	SA0086	SA0103	SA0127	SA0131	SA0230	SA0250	SA0277	SA0021	SA0031	SA0096	SA0162	SA0214
Cells per mm^2	9.48	5.34	2.68	5.32	2.48	4.67	16.29	5.38	11.4	1.75	2.54	5.55	5.36	1.75	3.09	9.38
Prefrontal HALO																
	SA0051	SA0062	SA0067	SA0076	SA0086	SA0103	SA0127	SA0131	SA0230	SA0250	SA0277	SA0021	SA0031	SA0096	SA0162	SA0214
Cells per mm^2	7.9	2.04	2.03	4.44	2.14	2.87		6.02	57.15		11.4	6.47	3.12	1.1	12.34	34.35

Striatum HALO					PD								Controls			
	SA0051	SA0062	SA0067	SA0076	SA0086	SA0103	SA0127	SA0131	SA0230	SA0250	SA0277	SA0021	SA0031	SA0096	SA0162	SA0214
Cells per mm^2		8.49	12.19	9.47	6.33	13.32	12.67	11.39	16.58	2.35	7.7	16.77	13.88		4.9	8.4
Striatum ImageJ																
	SA0051	SA0062	SA0067	SA0076	SA0086	SA0103	SA0127	SA0131	SA0230	SA0250	SA0277	SA0021	SA0031	SA0096	SA0162	SA0214
Cells per mm^2	29.54	9.57	11.89	13.9	6.5	11.7	19.02	14.03	13.19	7.02	8.6	11.32	19.01	8.22	4.8	14.79